

A study of the uppermost inner core from $PKKP$ and $P'P'$ differential traveltimes

Sebastian Rost¹ and Edward J. Garnero²

¹Centre of the Study of Imaging and Dynamics of the Earth, University of California Santa Cruz, Santa Cruz, CA 95064, USA. E-mail: srost@es.ucsc.edu

²Department of Geological Sciences, Arizona State University, Tempe, AZ 85287, USA

Accepted 2003 September 25. Received 2003 May 20; in original form 2002 September 30

SUMMARY

We have assembled a data set of $PKKP_{df}-PKKP_{bc}$ ($PKKP_{df-bc}$) and $PKPPKP_{df}-PKKP_{bc}$ differential traveltimes. This data set is used to study the Earth's uppermost inner core in the western hemisphere. Data from the eastern Pacific are recorded at the Canadian Yellowknife array and travel through the inner core twice, once perpendicular to the Earth's rotation axis and once parallel to the rotation axis. Our polar paths sample a similar region to paths from the South Sandwich Islands to Alaska, an important path geometry for inner core anisotropy studies. Our data set has the potential to be an independent source of information on the structure of the inner core, and to be a good supplement to past PKP studies. Differential time residuals (relative to isotropic inner core models) of up to several seconds are found. The differential traveltimes show significant scatter (up to 6 s) making it difficult to attribute them to inner core anisotropy alone. Alternatively, strong heterogeneity in the inner core and along the mantle paths may contribute to observations.

Key words: anisotropy, array, Earth's core, inner core, seismology.

1 INTRODUCTION

The radial isotropic P -wave structure of the inner core is well known from body waves and normal modes (Stark *et al.* 1986; Masters & Shearer 1990). However, the less-well constrained aspherical structure of the core is important for our understanding of the geodynamo and the chemistry and dynamics of the core. P -wave velocity anisotropy for Earth's inner core was first proposed over 15 yr ago based on anomalous body wave traveltimes and normal mode splitting data (Morelli *et al.* 1986; Woodhouse *et al.* 1986). An increasing number of structures in the inner core has been detected in recent years including cylindrical anisotropy in the inner core (see Song 1997; Creager 2000; Tromp 2001 for reviews), topography on the inner core boundary (Souriau & Souriau 1989), small scatterers within the inner core (Vidale & Earle 2000), hemispheric differences of anisotropy (Tanaka & Hamaguchi 1997; Creager 2000) and hemispheric changes of velocity and attenuation (Niu & Wen 2001; Wen & Niu 2002). Inner core anisotropy (ICA) is now widely accepted, with variations in cited magnitudes of around 1–3.5 per cent (see Song 1997; Creager 2000; Tromp 2001 for reviews) with the fast direction roughly aligned with the rotation axis of the Earth. Recent mineral-physical results show that the expected high pressure form of iron in the inner core can provide a high level of anisotropy (Steinle-Neumann *et al.* 2001) without the need to align unreasonable amounts of Fe with Earth's rotation axis.

Differential traveltimes of the seismic phases PKP_{ab} or PKP_{bc} , core phases that travel through the outer core only, and PKP_{df} ,

a core phase that travels through the inner core, have been widely used in inner core body wave studies. A strong difference is apparent between PKP traveltimes for equatorial and polar paths, with a faster direction of P -wave propagation roughly parallel to Earth's rotation axis. A notable difference between the quasi-eastern (i.e. 40°E–160°E) and western hemispheres, with stronger anisotropy in the western hemisphere has also been demonstrated (Tanaka & Hamaguchi 1997; Creager 2000). Different mechanisms to provide the hemispheric difference have been proposed explaining ICA by texturing during crystallization of iron during inner core growth (Bergman 1997) or subsequent to solidification as a result of plastic deformation (Buffett & Wenk 2001). Additionally, depth dependence of ICA has been noted: the uppermost 50–150 km of the western hemisphere inner core is compatible with an absence of anisotropy (Song & Helmberger 1995, 1998; Ouzounis & Creager 2001; Song & Xu 2002) and recent studies with a better global data coverage see evidence for a thinner isotropic region on the top of the inner core in the western hemisphere than in the eastern hemisphere (Niu & Wen 2001; Wen & Niu 2002). The shallowest inner core, however, is not as well sampled as the deeper inner core by turning rays in past studies (Niu & Wen 2001; Ouzounis & Creager 2001). Below we describe seismic wave paths that help us to address the shallower structure of the inner core.

Many of the inner core polar path geometries come from the South Sandwich Islands (SSI) earthquakes recorded at Alaskan stations. It is important to assess possible contributions to traveltime and

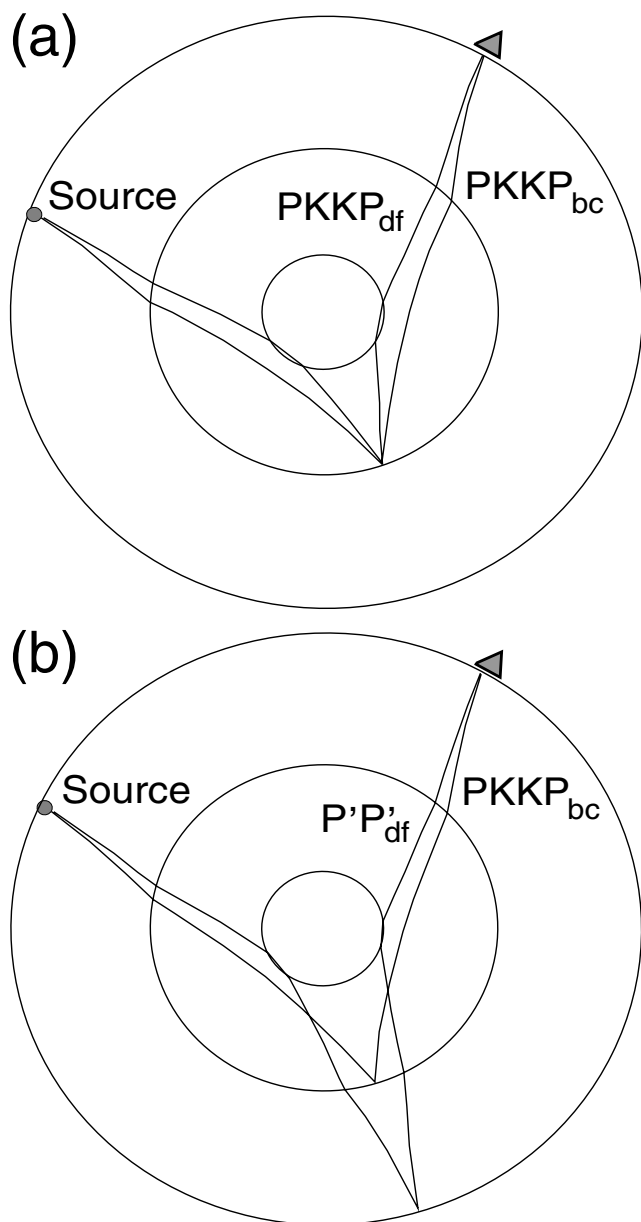


Figure 1. Ray-paths of $PKKP_{df}$, $PKKP_{bc}$ (a) and $PKKP_{bc}$ and $PKPPKP_{df}$ ($P'P'_{df}$) (b) through the radial Earth model ak135 (Kennett *et al.* 1995). All phases travel along the major arc of the great circle path. The epicentral distance range for events used in this study is $\sim 90^\circ - \sim 115^\circ$.

waveform variations from lower mantle or core–mantle boundary (CMB) structure (e.g. Bréger *et al.* 2000a; Creager 2000; Song 2000). We present an independent data set to study the anisotropy of the inner core: differential traveltimes of $PKKP_{df} - PKKP_{bc}$ ($PKKP_{df-bc}$) and $PKPPKP_{df}$ ($P'P'_{df}$, Lehmann 1936)– $PKKP_{bc}$, phases that travel twice through the inner core and are reflected once at the CMB or the surface, respectively (Fig. 1). Using differential traveltimes greatly reduces the effects of hypocentral uncertainties and lateral variations in crustal and upper-mantle structure. The second inner core segment (receiver side) of $PKKP$ and $P'P'$ for our path geometry is nearly parallel to the Earth's rotation axis, with similar sampling of the inner core to the often used SSI–AK (South Sandwich Islands to Alaska) PKP corridor beneath the western and central Atlantic. As a result of the different path geometries our

$PKKP$ and $P'P'$ phases sample the mantle and especially the heterogeneous CMB at different points from the widely used PKP phases from SSI to Alaska.

In what follows, we present our data stacking procedure and larger differential traveltime anomalies than predicted by recent models of ICA. For the distance range of our $PKKP_{df}$ and $P'P'_{df}$ data, ray paths bottom in the uppermost 100 km of the inner core (source–receiver geometry limitations prevent deeper inner core analysis using $PKKP$ or $P'P'$ for our ray path geometry). This indicates that either the outermost inner core is (at least locally) strongly anisotropic or heterogeneous, or structure somewhere else along the path is a contributing source of contamination. Both possibilities are explored, with a focus on the inner core beneath the Atlantic, which overlaps the SSI–AK corridor.

2 DATA SET

Earthquakes from the southwest and western Pacific, recorded at the short-period, small-aperture Yellowknife array (YKA) in northern Canada are studied (Fig. 2). YKA consists of 18 vertical component stations in a cross-shaped configuration with an aperture of 20 km. The interstation spacing is 2.5 km and the array shows very small slowness and backazimuth deviations due to a homogeneous, horizontal layering beneath the array (Manchee & Weichert 1968; Bondár *et al.* 1999). The dominant period of the seismometers is ~ 1 s. YKA is especially well suited to study low amplitude, high frequency P -waves. Events recorded between 1989 September and 1996 June are used in this study. Only events with magnitude $m_b > 5.5$ are used to guarantee a good signal-to-noise ratio. Many events recorded at YKA show very large $PKKP$ arrivals well above the noise level making the identification relatively easy. Events with $pPKKP_{bc}$ in the $PKKP_{df}$ arrival time window are excluded from this study.

We use stacking procedures to enhance the signal-to-noise ratio of the subtle signals from the inner core and to identify the $PKKP$ (and $P'P'$) branches by their slowness. We employ fourth-root vespagrams (Davies *et al.* 1971; Muirhead & Datt 1976; McFadden *et al.* 1986) and third-power phase-weighted-stack (PWS, Schimmel & Paulssen 1997) which highlights their slowness difference. Both stacking mechanisms are non-linear with smaller waveform distortion due to non-linearity for PWS (Schimmel & Paulssen 1997). The slowness difference of $PKKP_{bc}$ and $PKKP_{df}$ is between 0.8 and 1.5 s deg^{-1} (Fig. 3) depending on the epicentral distance range ($\sim 90^\circ - \sim 115^\circ$ in this study). Using YKA we are able to resolve slowness differences of 0.15 s deg^{-1} in our stacks and are therefore able to separate $PKKP_{bc}$ and $PKKP_{df}$ even with small differential traveltimes. The differential traveltime of the two branches of $PKKP$ is small and $PKKP_{df}$ often arrives in the $PKKP_{bc}$ -coda, therefore a clear identification of the different branches is vital. $PKKP_{df}$ and $P'P'_{df}$ in our data set turn less than 100 and 50 km beneath the inner core boundary, respectively. Thus, this study can only address structure in the outermost inner core.

3 DIFFERENTIAL TRAVELTIMES

We measured $PKKP_{df-bc}$ from 59 events, and $P'P'_{df} - PKKP_{bc}$ from 49 events. Recordings of 7 events have been used for both $PKKP_{df-bc}$ and $P'P'_{df} - PKKP_{bc}$ measurements. Differential times were measured from the vespagrams with a precision of 0.2 s (see Figs 4–6). The results of N th-root stacking and PWS are very similar. The vespagrams in Fig. 4 show various core phases arriving at their appropriate slownesses. Zooming in on the $PKKP$ wave group

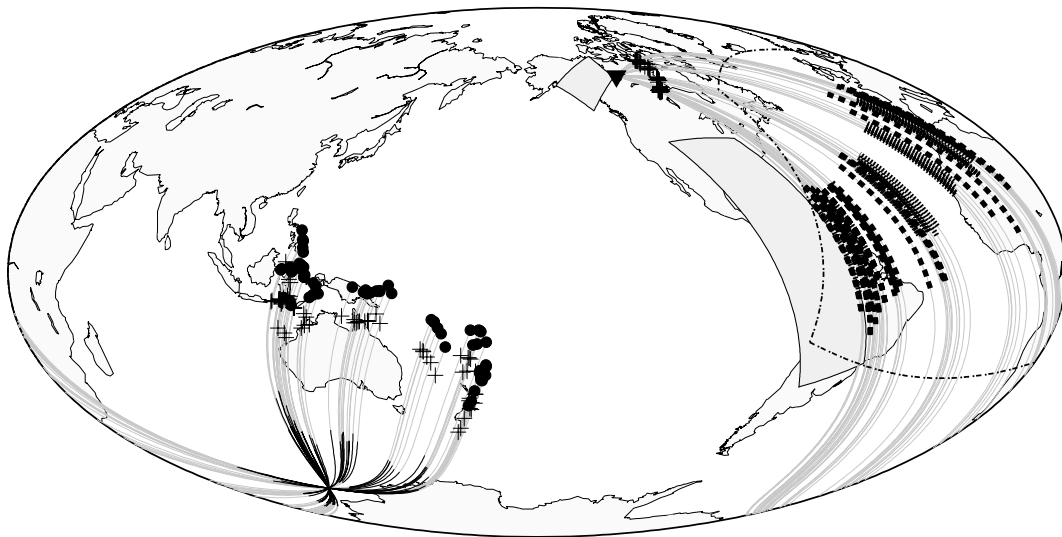


Figure 2. (a) Earthquakes (circles) and station YKA (triangle) with raypaths in Hammer projection. The crosses mark the entrance and exit points of the raypaths into the outer core at the CMB. The rays travel through the inner core twice. The equatorial inner core segments for PKKP and P'P' are shown as thin lines south of the earthquake source region. The thick line segments in and around the Atlantic are the polar inner core paths for P'P' (dotted) and PKKP (dashed). The complete raypath is shown in grey. The dash-dotted region surrounding most of the Atlantic is the region enlarged in Fig. 8. The grey-shaded areas beneath South- and Central America and Alaska approximately mark the region of the inner core and mantle probed by the SSI-AK path, respectively.

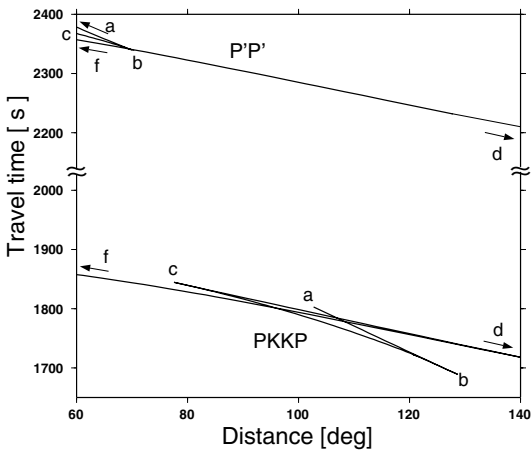


Figure 3. PKKP and P'P' traveltimes in the epicentral distance range of 60°–120°. Given is absolute traveltimes. In the distance range studied here (90°–120°) PKKP_{bc} and PKKP_{df} is observed. PKKP_{ab} is observed between ~100° and 120°. P'P'_{bc}, the reference phase to P'P'_{df} with a very similar ray-path cannot be observed for the epicentral distances of the data, and we therefore use PKKP_{bc} instead.

allows clear identification of the *ab*, *bc* and *df* branches, particularly when considering slowness differences. The difference between the slowness of PKKP_{bc} and PKKP_{df} is at least 0.8 s deg⁻¹ for the distance range (epicentral distance ~90° – ~115°) studied. This slowness difference can be easily resolved using YKA. When looking at individual stacked traces for slownesses appropriate for specific PKKP arrivals (Fig. 6), we see clear identification of *bc* and *df*. A careful investigation of the raw seismograms (Fig. 6a) shows that no *bc*-coda contamination of *df* is present. P'P'_{df} can be detected as impulsive onsets in many raw seismograms and the identification is easy. Fig. 5 displays a fourth-root vespagram of the event shown in Fig. 4(a) including the P'P' time window. Traveltimes for P'P'_{df} can easily be picked from the fourth-root vespagrams.

Fig. 6(a) shows bandpass filtered seismograms for one event (07-APR-1992_03:37) in Banda Sea. The corner frequencies of the fourth-order bandpass are 0.5 and 1.4 Hz. Arrivals with correct traveltimes for PKKP_{bc}, PKKP_{ab} and PKKP_{df} are clearly visible but without slowness information a definite identification of the phases is difficult. Figs 6(b) and (c) show the PWS trace and the *N*th-root stack (*N* = 4) trace for the appropriate PKKP_{bc} and PKKP_{df} slowness, respectively. The differences of the results of the two techniques are marginal and the measurements of the differential traveltimes can be done with high precision. As a result of the similarity of *N*th-root and PWS results we show differential traveltimes for *N*th-root stacking only. Waveform analyses with our stacked data are not possible due to distortion of the non-linear stacking mechanism (McFadden *et al.* 1986; Schimmel & Paulssen 1997), but PKKP_{df} (and P'P'_{df}) and PKKP_{bc} waveforms are often visible in the raw seismograms and in linear stacks (cf. Fig. 6). We find that the waveforms of the two phases are stable and very similar, although the *df*-phases show lower frequencies due to the attenuating structure of the inner core.

Traveltimes anomalies ($\Delta\tau$) are calculated from observed minus predicted differential times, where predictions are from the radial Earth model ak135 (Kennett *et al.* 1995), which assumes an isotropic inner core. We rate every traveltimes measurement with a quality between 1 (best) and 4 (worst), depending on the signal amplitude and vespagram quality. Only measurements with ratings of 1 or 2 are considered in further analyses. Numerous events show one arrival (*bc* or *df*) only and were discarded from our analysis. Remaining events show clear and sharp *df* and *bc* onsets in the fourth-root vespagrams with the appropriate slowness difference between the phases. To minimize mantle contributions to P'P'_{df} – PKKP_{bc}, their residuals are corrected for aspherical *P*-wave structure (van der Hilst *et al.* 1997; Káráson & van der Hilst 2001) (Fig. 7). We also use a combined model, that utilizes *D'* velocities from Tkalčić *et al.* (2002) and the overlying mantle from the Káráson & van der Hilst (2001) model. The influence of these corrections is relatively small, with maximum contributions from –0.9 to 0 s for

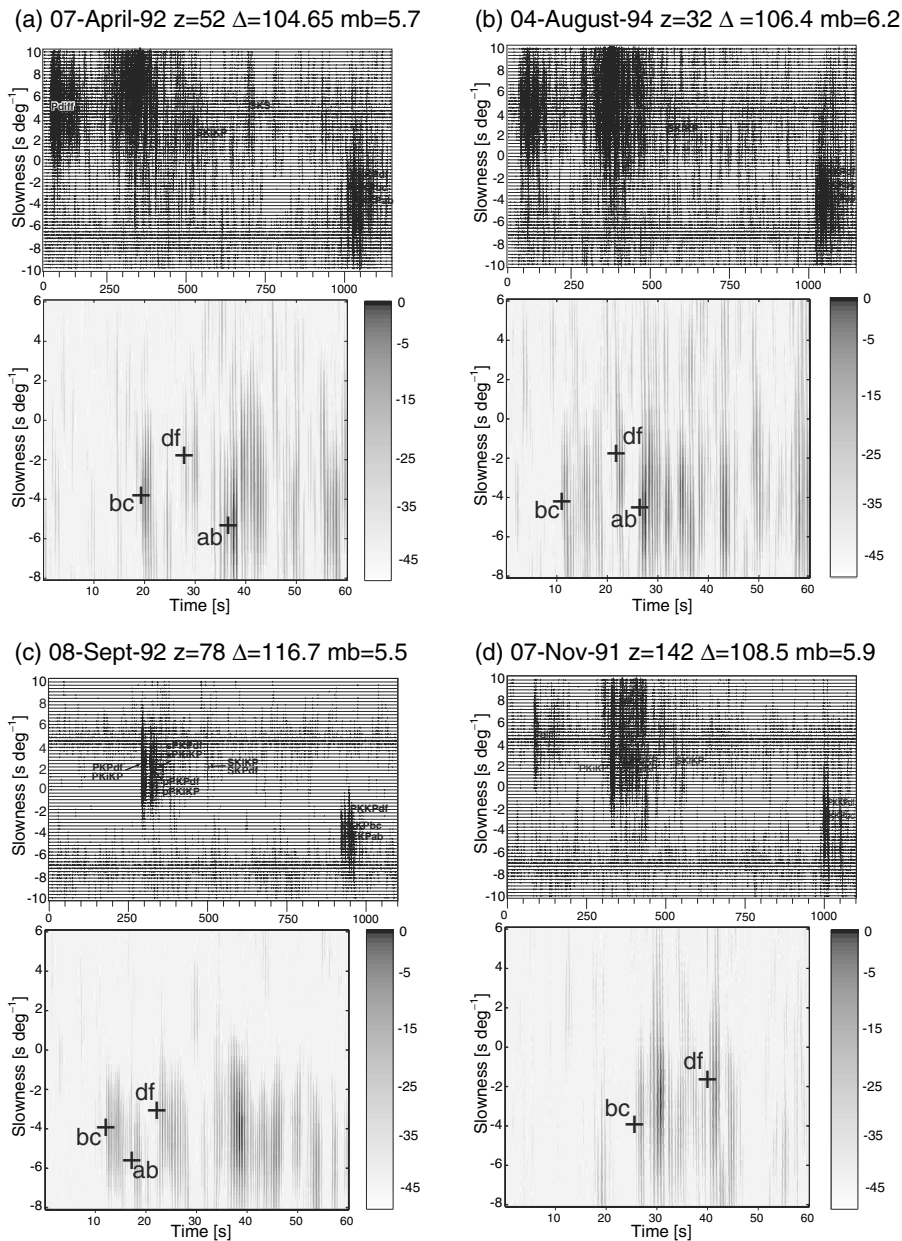


Figure 4. Fourth-root vespagrams for four example events (a) 07-APR-1992 UTC 03:37, (b) 04-AUG-1994 UTC 22:15, (c) 08-SEP-1992 UTC 13:50, (d) 07-NOV-1992 UTC 09:21. The upper panels show a vespagram with slownesses from -10 s deg^{-1} (major arc path) to 10 s deg^{-1} (minor arc path) in the time window between *P* and *PKKP* ($\sim 1200 \text{ s}$). Δ indicates the epicentral distance along the minor arc, z is the depth of the events in km and the body wave magnitude is given by mb. The dominant phases in the vespagrams are marked with the appropriate slowness and traveltime. *PKKP* is observable as strong phase near the end of the time windows. Lower panels show a zoom into the *PKKP* time window. The slowness range is shown from -8 to 6 s deg^{-1} . The crosses mark the theoretical slowness of *PKKP*_{bc}, *PKKP*_{ab} (when observable) and *PKKP*_{df}. The slowness difference between *PKKP*_{bc} and *PKKP*_{df} can be clearly observed in these vespagrams.

our path geometries. The largest traveltime anomaly is visible for phases travelling through the low-velocity anomaly beneath Africa (Ritsema *et al.* 1998). Using the combined model does not change the traveltime predictions through the tomographic models much. We experimented with increasing the variations of *P*-velocity in D' , which gave the expected results of stronger predicted residuals (e.g. multiplying the deepest layer in the Káráson & van der Hilst (2001) model by a factor of two results in a maximum predicted residual of approximately -1.6 s).

ICA perturbs raypaths since the inner core segments of, for example, *PKKP*_{df} sample different velocities along polar versus equatorial regions. Traveltime perturbations produced from this asymmetry are not currently taken into account, and we note this may influence conclusions regarding magnitude of anisotropy (here and past studies).

Fig. 8 shows the resulting differential traveltimes for *PKKP* and *P'P'* projected on to the polar inner core path. The region sampled by our data set lies to the east of the important SSI–AK path used

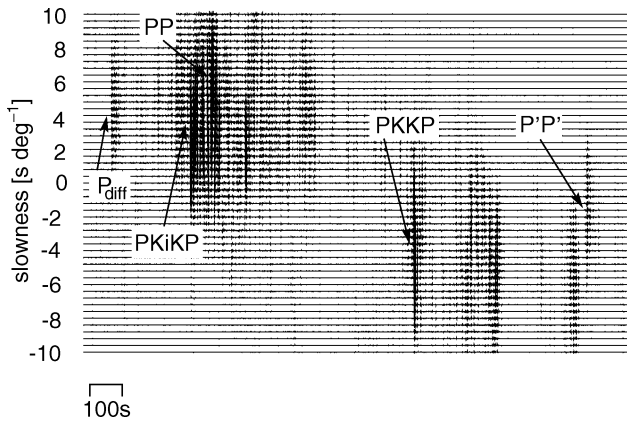


Figure 5. Fourth-root vespagram for the event shown in Fig. 4a but the whole time window between P_{diff} and $P'P'$ is shown. The epicentral distance is 112° , therefore P_{diff} is weak. $P'P'$ is small but can be easily identified as impulsive onset in the fourth-root vespagram. The slowness range shown is -10 s deg^{-1} (major arc arrival) to 10 s deg^{-1} (minor arc arrival).

in past *PKP* differential traveltime studies. The $P'P'$ traveltimes are corrected for mantle structure for the tomographic model by Káráson & van der Hilst (2001). $P'P'_{df}$ (dotted outline) shows generally shorter inner core segments than $PKKP_{df}$ (solid outline). The measured differential traveltime anomalies neither show any large-scale pattern with latitude nor longitude of the df turning point in the inner core along the polar path (Figs 9 and 10). The range of scatter in the differential traveltime anomalies is very high ($\sim 5\text{--}6 \text{ s}$) but is similar to the *PKP* differential times reported for the SSI–AK corridor (e.g. fig. 3 of Tkalčić *et al.* 2002). We also see no obvious dependence of the differential traveltime anomaly with inner core turning point depths (Fig. 11). $P'P'_{df}$ samples only the uppermost 50 km and $PKKP_{df}$ the uppermost 100 km of the inner core. This region of the inner core is found to be isotropic in previous studies (e.g. Niu & Wen 2001; Wen & Niu 2002). Fig. 12 shows differential traveltime residuals for $PKKP_{df} - PKKP_{bc}$ ($\Delta\tau_{PKKP}$) and $PKPPKP_{df} - PKKP_{bc}$ ($\Delta\tau_{P'P'}$). To compare paths with different inner core path-lengths we show traveltime residuals normalized by the path-length (in $^\circ$) of the df branch in the inner core in Fig. 12c and d. The traveltime residuals are shown with respect to the angle between the inner core path and the Earth's rotation axis ξ (Shearer & Toy 1991; Su & Dziewonski 1995) for both the polar and equatorial path of $PKKP_{df}$ and $P'P'_{df}$. Also shown are differential traveltime residual predictions for the same path configurations for an anisotropic inner core model (Creager 1992; Song 1997). We use this model although newer studies show that the uppermost inner core is isotropic (Shearer 1994; Song & Helmberger 1995; Creager 2000; Niu & Wen 2001; Song & Xu 2002; Wen & Niu 2002). Neither the path-normalized nor the un-normalized differential traveltime residuals agree with the predictions for the anisotropic inner core model by Creager (1992). Interpreting (ξ , $\Delta\tau$) for our data is complicated by the fact that the inner core is sampled by two df legs, each with different ξ . We assume that the influence of the equatorial path on the traveltimes is small. This is supported by *PKP* $_{df-bc}$ traveltimes that show that near equatorial *PKP* $_{df-bc}$ times show no traveltime anomaly for $\xi \geq 55^\circ$ (e.g. see Creager 2000). Here we study $\Delta\tau_{PKKP}$ and $\Delta\tau_{P'P'}$ for polar and near polar paths with ξ smaller than 46° .

$\Delta\tau_{PKKP}$ (not normalized), is as low as -6.2 s . The differential traveltime anomalies are largely due to fast $PKKP_{df}$ arrivals, rather

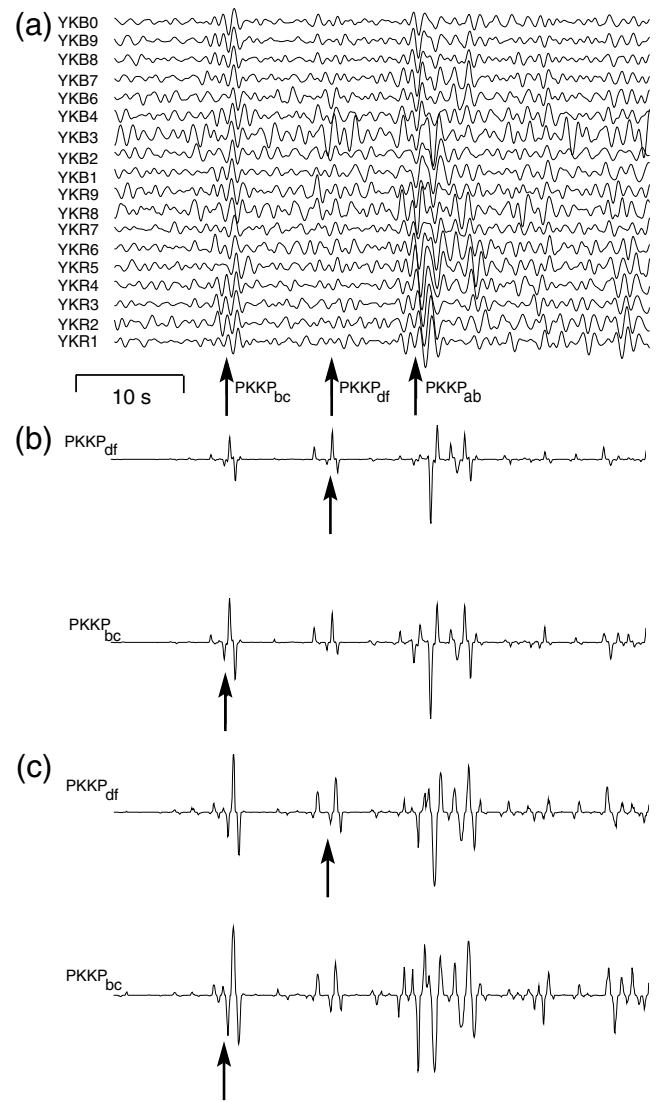


Figure 6. (a) Bandpass filtered seismograms of *PKKP* time windows. A weak onset with $PKKP_{df}$ arrival time is visible between the strong $PKKP_{bc}$ and $PKKP_{ab}$ branches. (b) Phase weighted stack traces for $PKKP_{bc}$ and $PKKP_{df}$ slowness. The arrivals are marked by the arrows. (c) Fourth-root stack trace. The slowness resolution is less strong than in (b). The arrivals are marked as in (b).

than slow $PKKP_{bc}$ arrivals. In fact, 22 of our 32 $\Delta\tau_{PKKP}$ residuals are negative, with the majority between -2 and -4 s (17 measurements). No apparent trend of $\Delta\tau_{PKKP}$ with ξ is visible. Although the interpretation of $P'P'_{df}$ is more complicated due to the long additional mantle path, $\Delta\tau_{P'P'}$ residuals behave similarly to $\Delta\tau_{PKKP}$: residuals are as low as -6 s with 27 of the 35 observations being negative. The negative $\Delta\tau_{P'P'}$ times are also mostly due to fast $P'P'_{df}$ arrivals possibly from inner core structure. $\Delta\tau_{P'P'}$ residuals are evenly distributed in the -2 to -6 s range; a few of our $\Delta\tau_{P'P'}$ data show no anomaly at all (see Fig. 12).

Nonetheless, some trends in the geographical patterns of $\Delta\tau$ (see, e.g., Fig. 8) are present. We observe a reduction of the differential traveltime residuals both for $PKKP_{df} - PKKP_{bc}$ and $P'P'_{df} - PKKP_{bc}$ in different latitude and longitude bands. The reduction from -70° to -50° longitude and 5° to 12° latitude is the most pronounced, but it can be also observed in other bands such as -50° to -30° longitude and 15° to 25° latitude. We cannot associate the

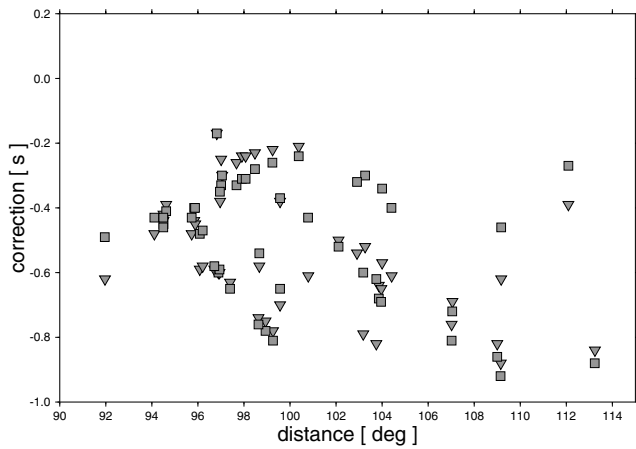


Figure 7. Traveltime correction through 3-D tomographic mantle models by Káráson & van der Hilst (2001) (squares) and Tkalčić *et al.* (2002) (triangles) for $P'P'_{df} - PKKP_{bc}$ versus source–receiver distance (see the text for details). Traveltime corrections are calculated for each source–receiver combination. The corrections due to laterally varying P -wave velocities in the mantle are small and differences in the predicted traveltime residuals for the two models used for our path geometry is small (normally less than 1.0 s).

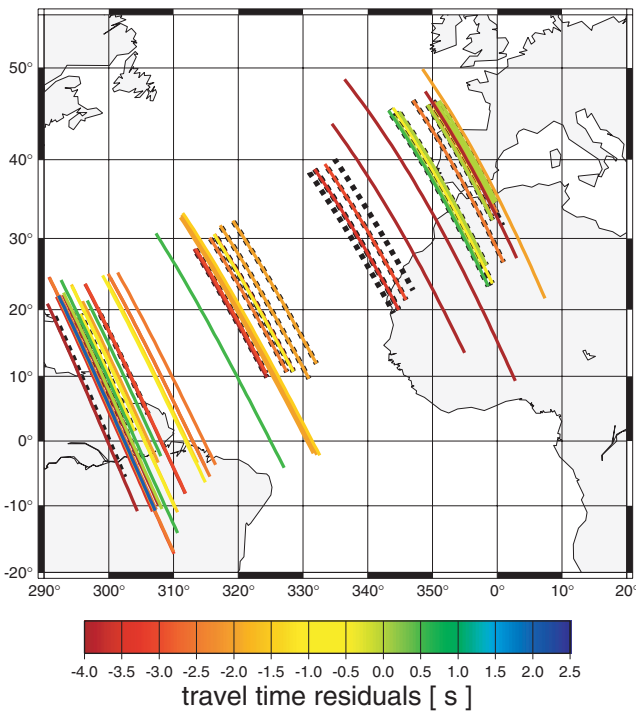


Figure 8. Differential traveltime residuals along polar inner core path. The residuals are relative to radial Earth model AK135 (Kennett *et al.* 1995). Solid outlines mark $PKKP_{df}$ paths and dotted outlines mark $P'P'_{df}$ paths through the inner core. The inner core beneath the central Atlantic in the region between South-America and North Africa can be studied. The region studied is just east of the region sampled by the prominent PKP path from the South Sandwich Islands to Alaska (compare Fig. 2).

slight geographic variation of differential traveltime residuals in Figs 9 and 10 with the turning depth of the df -phases (Fig. 11). The geographic patterns might be due to small-scale heterogeneity, either in the inner core or in the mantle. The changes of the traveltime

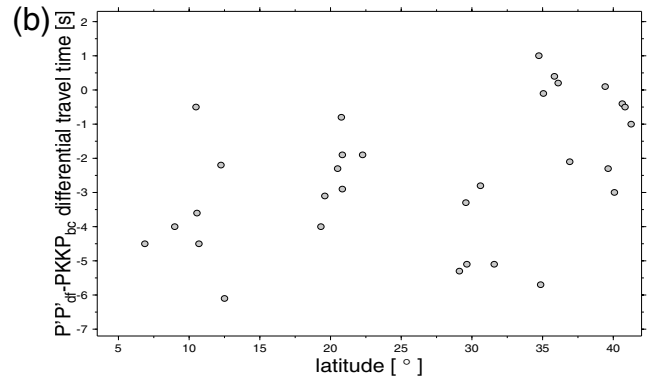
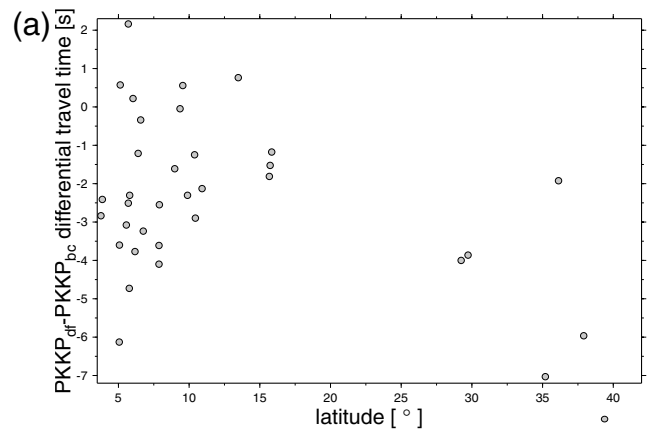


Figure 9. Differential traveltime residual versus latitude of the inner core turning point of the polar path. (a) Differential traveltime for $PKKP_{df} - PKKP_{bc}$ with respect to the latitude of the inner core turning point of the polar path of $PKKP$. (b) Same as (a) for $P'P'_{df} - PKKP_{bc}$. The differential traveltime residuals for $P'P'_{df} - PKKP_{bc}$ are corrected for mantle contributions from the tomographic model by Káráson & van der Hilst (2001).

anomaly are well above our picking error, but the data nonetheless show a lot of scatter. As we discuss below, this may be either due to lateral variations in ICA, inner core heterogeneity, or a non-inner core source.

4 DISCUSSION AND CONCLUSIONS

With the similar paths of $PKKP_{bc}$ and $PKKP_{df}$ in the mantle and the path of df through the inner core this phase pair should provide information on the structure of the uppermost inner core. The phase pair $PKKP_{bc}$ and $P'P'_{df}$ may be more problematic due to the long additional path of $P'P'$ through the mantle and the interaction of $P'P'$ with the heterogeneous zones at the CMB and in the upper-mantle. We are well aware that we cannot account for possible large amplitude heterogeneity at small-scales in the mantle by applying traveltime corrections from tomographic models that predominantly characterize Earth's long-wavelength heterogeneity. Nonetheless, the variability and scatter as shown in Figs 8–12 in our data are surprising.

Different factors might affect the differential traveltimes. Source mislocation, both laterally and in depth should have a small influence since using phase pairs mitigates the problem. Just as well, the paths of the phase pairs in the upper-mantle are very similar, so that traveltime variations along the upper-mantle paths should be small. Nonetheless, extreme upper-mantle structures, such as subduction

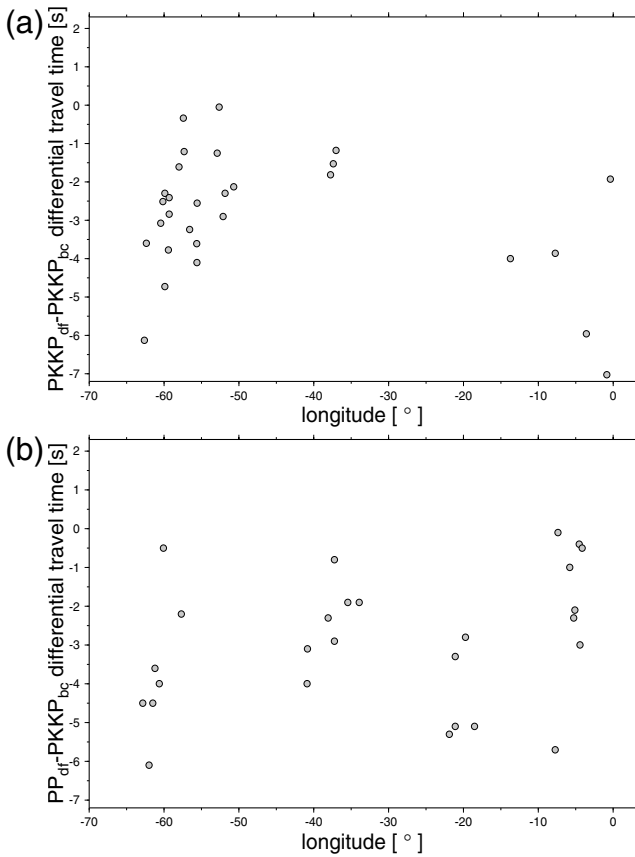


Figure 10. Differential traveltime residual versus longitude of the inner core turning point of the polar path. (a) Differential traveltime for $PKKP_{df} - PKKP_{bc}$ with respect to the longitude of the inner core turning point of the polar path of $PKKP$. (b) Same as (a) but for $P'P'_{df} - PKKP_{bc}$. The differential traveltime residuals for $P'P'_{df} - PKKP_{bc}$ are corrected for mantle contributions from the tomographic model by Kárason & van der Hilst (2001).

zones, could effect the differential traveltimes (Helffrich & Sacks 1994; Weber 1990).

Although the $PKKP_{df}$ and $PKKP_{bc}$ paths in the upper-mantle are very similar, they enter the outer core at locations several degrees apart. $PKKP$ travels through D' nearly vertically so that traveltime influences from heterogeneities should be small. Nonetheless it has been shown that the CMB contains large velocity reductions (Garnero *et al.* 1998) and strong heterogeneity on small scalelengths (Kito & Krüger 2001; Ni & Helmberger 2001; Rost & Revenaugh 2001, 2003). Although ultralow-velocity zones (ULVZ) are only up to tens of km thick they can influence traveltimes due to their large velocity reductions of up to 10 per cent. For $PKKP$, the CMB entry and exit areas close to source and receiver (Fig. 2) are north (and east) of Australia and beneath Canada, respectively. The area with most of the entry points near Australia has not been probed for ULVZ structure or they do not show ULVZ structure; the closely grouped core exit locations have been probed unsuccessfully for ULVZ structure (Garnero *et al.* 1998). The two additional CMB exit and entry points for $P'P'_{df}$ are located in the southern Atlantic and beneath southern Africa. Unfortunately, those areas have not been probed for ULVZ structure either. However, tomographic models show a strong slow anomaly in this region, especially in S -wave velocity (Grand 1994; Ritsema & van Heijst 2000), which might indicate

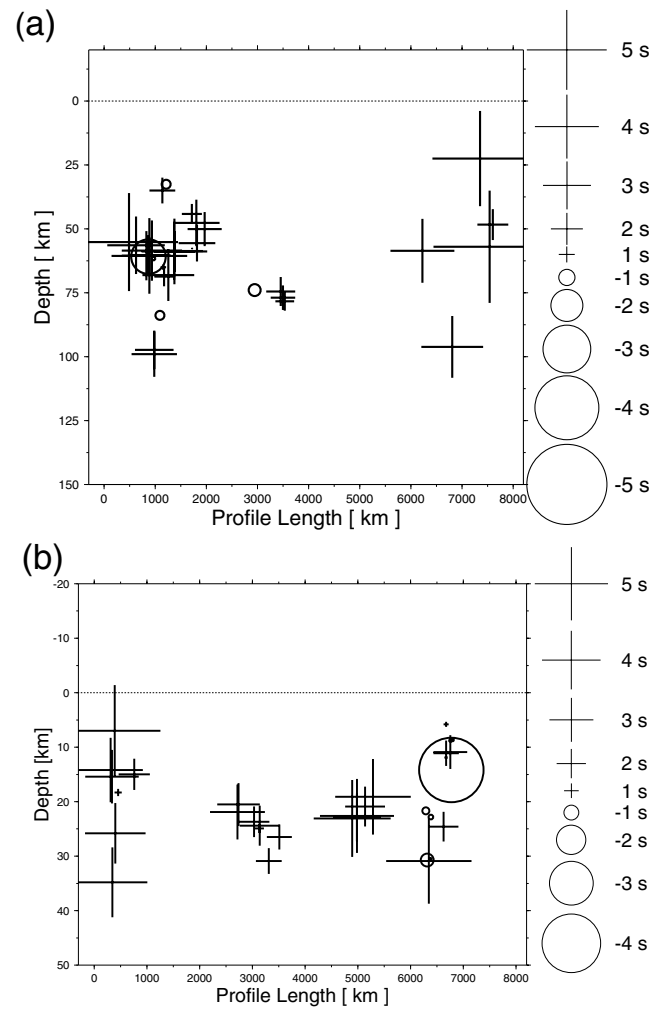


Figure 11. Differential traveltime residuals versus inner core turning depth for (a) $PKKP_{df} - bc$ and (b) $PKPPKP_{df} - PKKP_{bc}$. The maximum depth of the inner core turning point is shown along a West-East profile. The dashed line shows the depth of the inner core boundary. The symbol size indicates differential traveltime residuals.

strong heterogeneity close to the CMB not captured in its complete amplitude in the tomography models.

Lateral variations in outer core wave speed as the source for the scattering is unlikely since the outer core should be well mixed due to its low-viscosity and the short turnover time of core convection (Braginsky 1993; Loper 2000), although a recent study (Romanowicz *et al.* 2003) states that a 1 per cent faster velocity inside an outer core region roughly delimited by the inner core tangent cylinder allows a better fit to trends of $PKKP_{df}$ absolute traveltimes. The most anomalous (not normalized) predicted traveltimes for an anisotropic inner core model (Creager 1992; Song 1997) are around -2 s (corresponding to a maximum ICA of ~ 3 per cent) (Fig. 12); this is several seconds less than our observations. To explain our data, much stronger ICA is necessary (7–10 per cent). This is incompatible with other studies, in particular, those that have presented evidence for an isotropic outermost inner core (e.g. Shearer 1994; Song & Helmberger 1995; Garcia & Souriau 2000; Niu & Wen 2001; Ouzounis & Creager 2001; Song & Xu 2002; Wen & Niu 2002). Though we note that studies using normal modes are consistent with anisotropy throughout the inner core (e.g. see Tromp 1993; Durek & Romanowicz 1999).

A number of possibilities exist to explain our observations. To test the hypothesis that the scatter in our data might be due to our methods, we processed *PKP* phases from SSI to YKA with the same method applied to *PKKP*. We measured differential traveltimes between *PKP_{cd}* and *PKP_{df}*. The residuals ranged from -1.5 to 0.5 s, for an epicentral distance of 126° – 146° . The scatter in these results (~ 2 s) is much less than in *PKKP*. This range of scatter is similar to that of other studies using *PKP* (e.g. McSweeney *et al.* 1997; Wen & Niu 2002). The cross correlation technique (McSweeney *et al.* 1997) applied to the *PKP* data set leads to very similar differential traveltimes to those from our vespa technique, with a maximum of 0.2 s difference. Thus, scatter in the travel-time measurements from the vespa method is not due to the vespa approach. Hence, using slowness stacking, the *PKKP* and *P'P'* arrivals are coherently enhanced to be significantly out of the noise level (e.g. Figs 4 and 6), and accurate differential times can be extracted. This would not likely be possible using single seismogram methods that are routinely employed in *PKP* analyses, since *PKKP_{df}* is relatively weak. Additionally, using single seismograms a slowness discrimination between the *bc* and *df* branches of *PKKP* is not possible.

The paths for *PKKP_{bc}* and *PKKP_{df}* are very similar through most of the Earth. Nonetheless, they are separated by several degrees at the base of the mantle. We expect some contribution to our residuals from *D''* inhomogeneities, which may affect the *bc* and *df* branches differently (e.g. see Bréger *et al.* 2000a; Creager 2000). However, very large *D''* heterogeneity is required: to explain a 5 s residual, for

a 300 km thick *D''* layer, one of the *PKKP* branches must uniquely traverse a ~ 18 per cent anomaly (distributed over the entire 300 km thick *D''*) if restricted to a single core crossing location. For comparison, ultralow-velocity zones, regions of extreme deepest mantle heterogeneity, have been modelled with thicknesses less than 40–50 km, and *P*-wave reductions of 10 per cent (Garnero *et al.* 1998). If distributed over both the core entry and exit sides of the *df* or *bc* path (again, throughout a 300 km *D''*), a ~ 9 per cent velocity perturbation is necessary. For $\Delta\tau_{P'P'}$ residuals, if due to *D''* structure, velocity perturbations can be located along any combination of each of the 4 legs of *D''* crossings (e.g. requiring 18, 9 or 4.5 per cent heterogeneity for 1, 2 or 4 affected *P'P'* legs, respectively).

Another candidate location for unaccounted heterogeneity is the upper mantle, especially for *P'P'*. For the uppermost 300 km of the mantle a 4–5 per cent (2–2.5 per cent) velocity perturbation along one leg (two legs) is required to produce a 5 s contribution to residuals. Upper mantle structure may also affect *PKKP*, though it must be extremely short scale (laterally) as to not similarly perturb the neighbouring phase (separated by only a few km) used in the differential time (*PKKP_{bc}* and *PKKP_{df}*). Subduction zones might fulfil this criterion. Alternatively, structure somewhere between the CMB and the surface beneath the receiver may play a significant role in contributing to the SSI–AK anomalies cited in past studies (Bréger *et al.* 1999, 2000b; Romanowicz *et al.* 2003). Our paths beneath YKA are similar, but do not overlap the SSI–AK data (see Fig. 2). Thus, if receiver-side mantle structure is the source of large amplitude anomalies in our *PKKP* and past SSI–AK *PKP* data,

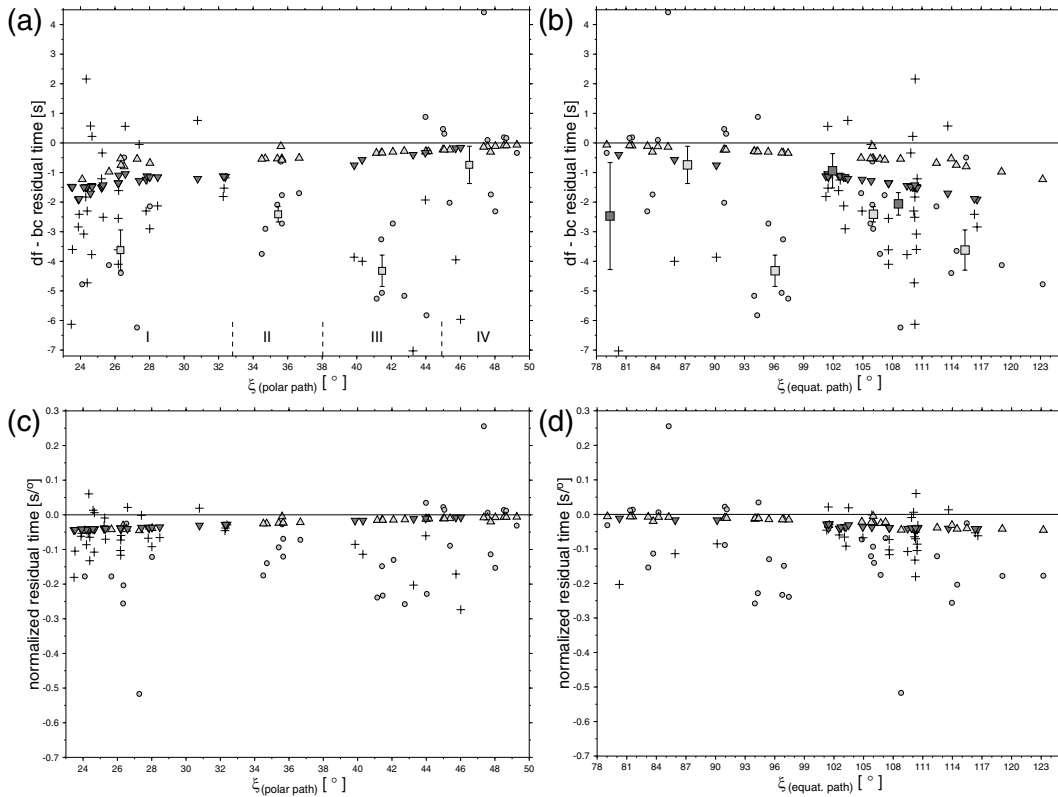


Figure 12. *PKKP_{df-bc}* (circles) and *PKPPKP_{df} - PKKP_{bc}* (crosses) traveltime anomalies versus angle ξ (Shearer & Toy 1991; Su & Dziewonski 1995) for polar (a) and equatorial paths (b). Traveltime anomalies are normalized with the respective inner core path-length for polar (c) and equatorial paths (d). Inverted triangles show traveltime predictions for *P'P'* for the same source–receiver combinations for an anisotropic inner core model (Creager 1992). Triangles show *PKKP* predictions. Squares in (a) and (b) show mean values regions (I–IV) in the profile as shown at the bottom of the figure.

then it extends over lateral scales of ~ 1800 km if in D' , or ~ 3200 km if in the upper few hundred km of the mantle beneath North America.

Our $\Delta\tau_{P'P'}$ residuals are admittedly more vulnerable to mantle contamination, since they contain two additional interactions with the CMB, D' , and mantle structure that are not probed by the reference phase $PKKP_{bc}$. To use $P'P'$ in inner core studies it might be better to use $P'P'_{bc}$ as a reference phase as has been shown by Bréger *et al.* (2000b). This is impossible for this study since $P'P'_{bc}$ does not exist in the epicentral distance range studied here (Fig. 3) and the use of $P'P'_{df}$ as an additional source of information for the same core region as for $PKKP_{df}$ would be impossible for shorter distances. Nonetheless, the variance for $\Delta\tau_{P'P'}$ is not as big as for $\Delta\tau_{PKKP}$ and a similar differential traveltime pattern as for $PKKP$ can be observed. Correcting $\Delta\tau_{P'P'}$ for smoothed and damped tomographic model predictions is a first step. However, the biggest challenge at present is the minimum scalelengths retrieved in tomographic inversions (where resolved), which are at best 500–1000 km. The hypothetical mantle perturbations presented above are perhaps unrealistically too large. Nonetheless, mantle heterogeneity undoubtedly contributes to the observed residuals, especially the scatter seen in Fig. 12.

Other factors may also contribute to the scatter in our data, but are not likely large, and our data are not able to resolve such contributions. These include CMB topography, ICB topography, and possible lateral variations in outer and inner core structure, including rigidity or mushy zones at the top of the inner and outer core. The observation of large scatter in near polar df paths is not unexpected. Bréger *et al.* (1999) propose a complex model of strong anisotropy, possibly associated with heterogeneity on short scalelengths to explain large excursions in $PKP_{bc} - PKP_{df}$ traveltime measurements. Similar to us they state that complex lowermost mantle structure could be an additional source of traveltime variability, although the large differential traveltimes observed in our study are hard to explain by structure only on one leg. Strong, small-scale structure on both, source and receiver side, might be necessary to explain our anomalous data as discussed above.

We summarize our main findings as follows.

(i) Differential times between the inner core branches of $PKKP$ and $P'P'$ permit new inner core analysis with good sampling in the outermost inner core.

(ii) Our differential times are consistent with past studies that note remarkably fast df waves through the inner core beneath the Atlantic, for pole-parallel wave paths, but lack a general trend of differential traveltimes with ξ .

(iii) The distance range of our data limits our analyses to the outermost 100 km of the inner core, therefore suggesting the presence of ICA (at least locally) in a region some studies have noted as isotropic. Alternatively, strong small-scale heterogeneity in the uppermost inner core (Singh *et al.* 2000; Vidale & Earle 2000) might significantly contribute to observed anomalies.

(iv) Assuming an isotropic uppermost inner core, our data require strong small-scale heterogeneity in the mantle, most likely at the core–mantle boundary.

(v) Uncertainties in contributions to observed residuals from poorly resolved mantle heterogeneity remain a challenge in this and future work.

The rapid variation of the differential traveltimes reported in this study can be understood as the result of a complex anisotropic structure and/or heterogeneity at the top of the inner core and/or mantle heterogeneity.

ACKNOWLEDGMENTS

Data from this study come from the Canadian Geological Survey. Figures were produced using GMT. This work was supported by the U.S. National Science Foundation CSEDI grant EAR-9905710 (SR and EG) and IGPP grant 02-GS-011 (SR) and CSIDE. We thank Thorne Lay and Justin Revenaugh and two anonymous reviewers for their helpful comments.

REFERENCES

- Bergman, M.I., 1997. Measurements of electric anisotropy due to solidification texturing and the implications for the Earth's inner core, *Nature*, **389**, 60–63.
- Bondár, I., North, R.G. & Beall, G., 1999. Teleseismic slowness-azimuth station corrections for the international monitoring system seismic network, *Bull. seism. Soc. Am.*, **89**, 989–1003.
- Braginsky, S.I., 1993. MAC oscillations of the hidden ocean of the core, *J. Geomagn. Geoelectr.*, **45**, 1517–1538.
- Bréger, L., Romanowicz, B. & Tkalčić, H., 1999. $PKP(BC - DF)$ traveltime residuals and short scale heterogeneity in the deep Earth, *Geophys. Res. Lett.*, **26**, 3169–3172.
- Bréger, L., Romanowicz, B. & Rousset, S., 2000a. New constraints on the structure of the inner core from $P'P'$, *Geophys. Res. Lett.*, **27**, 2781–2784.
- Bréger, L., Tkalčić, H. & Romanowicz, B., 2000b. The effect of D' on $PKP(AB-DF)$ travel time residuals and possible implications for inner core structure, *Earth planet. Sci. Lett.*, **175**, 133–143.
- Buffett, B.A. & Wenk, H.-R., 2001. Texturing of the Earth's inner core by Maxwell stresses, *Nature*, **413**, 60–63.
- Creager, K.C., 1992. Anisotropy of the inner core from differential travel times of the phases PKP and $PKIKP$, *Nature*, **356**, 309–314.
- Creager, K.C., 2000. Inner core anisotropy and rotation, in *Earth's Deep Interior: Mineral Physics and Tomography From the Atomic to the Global Scale*, *Geophysical Monograph 117*, pp. 89–114, eds Karato, S.-I., Forte, A.M., Liebermann, R.C., Masters, G. & Stixrude, L., American Geophysical Union, Washington DC.
- Davies, D., Kelly, E.J. & Filson, J.R., 1971. Vespa process for analysis of seismic signals, *Nature Phys. Sci.*, **232**, 8–13.
- Durek, J.J. & Romanowicz, B., 1999. Inner core anisotropy inferred by direct inversion of normal mode spectra, *Geophys. Res. Lett.*, **139**, 599–622.
- Garcia, R. & Souriau, A., 2000. Inner core anisotropy and heterogeneity level, *Geophys. Res. Lett.*, **27**, 3121–3124.
- Garnero, E.J., Revenaugh, J.S., Williams, Q., Lay, T. & Kellogg, L.H., 1998. Ultralow velocity zone at the core–mantle boundary, in *The Core–Mantle Boundary*, *Geodynamics Series 28*, pp. 319–334, eds M. Gurnis, et al., American Geophysical Union, Washington DC.
- Grand, S.P., 1994. Mantle shear structure beneath the Americas and surrounding oceans, *J. geophys. Res.*, **99**, 11 591–11 621.
- Helffrich, G. & Sacks, S., 1994. Scatter and bias in differential PKP travel times and implications for mantle and core phenomena, *Geophys. Res. Lett.*, **21**, 2167–2170.
- Kárason, H. & van der Hilst, R.D., 2001. Tomographic imaging of the lowermost mantle with differential times of refracted and diffracted core phases (PKP , P_{diff}), *J. geophys. Res.*, **106**, 6569–6587.
- Kennett, B.L.N., Engdahl, E.R. & Buland, R., 1995. Constraints on seismic velocities in the Earth from travel times, *Geophys. Res. Lett.*, **122**, 108–124.
- Kito, K. & Krüger, F., 2001. Heterogeneities in D' beneath the southwestern Pacific inferred from scattered and reflected, P -waves, *Geophys. Res. Lett.*, **28**, 2545–2548.
- Lehmann, I., 1936. P' , *Publ. Bur. Cent. Seism. Int. A*, **14**, 87–115.
- Loper, D.E., 2000. A model of the dynamical structure of Earth's outer core, *Phys. Earth planet. Inter.*, **117**, 179–196.
- McFadden, P.L., Drummond, B.J. & Kravis, S., 1986. The N th-root stack: theory, applications and examples, *Geophysics* **51**, 1879–1892.

- McSweeney, T.J., Creager, K.C. & Merrill, R.T., 1997. Depth extent of inner-core seismic anisotropy and implications for geomagnetism, *Phys. Earth planet. Inter.*, **101**, 131–156.
- Manchee, E.B. & Weichert, D.H., 1968. Epicentral uncertainties and detection probabilities from the Yellowknife seismic array data, *Bull. seism. Soc. Am.*, **58**, 1359–1377.
- Masters, T.G. & Shearer, P.M., 1990. Summary of seismological constraints in the structure of Earth's core, *J. geophys. Res.*, **95**, 21 691–21 695.
- Morelli, A., A.M. Dziewonski & Woodhouse, J.H., 1986. Anisotropy of the core inferred from *PKiKP* travel times, *Geophys. Res. Lett.*, **13**, 1545–1548.
- Muirhead, K.J. & Datt, R., 1976. The *N*-th root process applied to seismic array data, *Geophys. J. R. astr. Soc.*, **47**, 197–210.
- Ni, S. & Helmberger, D.V., 2001. Probing an ultra-low velocity zone at the core mantle boundary with *P* and *S* waves, *Geophys. Res. Lett.*, **28**, 2345–2348.
- Niu, F. & Wen, L., 2001. Hemispheric variations in seismic velocity at the top of the Earth's inner core, *Nature*, **410**, 1081–1084.
- Ouzounis, A. & Creager, K.C., 2001. Isotropy overlying anisotropy at the top of the inner core, *Geophys. Res. Lett.*, **28**, 4331–4334.
- Ritsema, J. & van Heijst, H.J., 2000. Seismic imaging of structural heterogeneity in Earth's mantle: evidence for large-scale mantle flow, *Sci. Progr.*, **83**, 243–259.
- Ritsema, J., Ni, S., Helmberger, D.V. & Crotwell, H.P., 1998. Evidence for strong shear wave velocity reductions and velocity gradients in the lower mantle beneath Africa, *Geophys. Res. Lett.*, **25**, 4245–4247.
- Romanowicz, B., Tkalčić, H. & Bréger, L., 2003. On the origin of complexity in *PKP* travel time data, in: *Earth's Core: Dynamics, Structure, Rotation, Geodynamics Series 31*, pp. 31–44, eds Dehant, V., et al American Geophysical Union, Washington, DC.
- Rost, S. & Revenaugh, J., 2001. Seismic detection of rigid zones at the top of the core, *Nature*, **294**, 1911–1914.
- Rost, S. & Revenaugh, J., 2003. Small-scale ultra-low velocity zone structure imaged by *ScP*, *J. geophys. Res.*, **108**, 10.1028/2001JB001 627.
- Schimmel, M. & Paulssen, H., 1997. Noise reduction and detection of weak, coherent signals through phase-weighted stacks, *Geophys. Res. Lett.*, **130**, 497–505.
- Shearer, P.M., 1994. Constraints on inner core anisotropy from *ISC PKP(DF)* travel times, *J. geophys. Res.*, **99**, 19 647–19 659.
- Shearer, P.M. & Toy, K.M., 1991. *PKP(BC)* versus *PKP(DF)* differential travel times and aspherical structure in the Earth's inner core, *J. geophys. Res.*, **96**, 2233–2247.
- Singh, S.C., Taylor, M.A.J. & Montagner, J.P., 2000. On the presence of liquid in Earth's inner core, *Science*, **287**, 2471–2474.
- Song, X., 1997. Anisotropy of the Earth's inner core, *Rev. Geophys.*, **35**, 297–313.
- Song, X., 2000. Joint inversion for inner core rotation, inner core anisotropy, and mantle heterogeneity, *J. geophys. Res.*, **105**, 7931–7943.
- Song, X. & Helmberger, D.V., 1995. Depth dependence of anisotropy of Earth's inner core, *J. geophys. Res.*, **100**, 9805–9816.
- Song, X. & Helmberger, D.V., 1998. Seismic evidence for an inner core transition zone, *Science*, **282**, 924–927.
- Song, X. & Xu, X., 2002. Inner core transition zone and anomalous *PKP(DF)* waveforms from polar paths, *Geophys. Res. Lett.*, **29**(4), 1042, doi: 10.1029/2001GL013822.
- Souriau, A. & Souriau, M., 1989. Ellipticity and density an the inner core boundary from subcritical *PKiKP* and *PcP* data, *Geophys. Res. Lett.*, **98**, 39–54.
- Stark, P.B., Parker, R.L., Masters, G. & Orcutt, J.A., 1986. Strict bounds on seismic velocity in the spherical Earth, *J. geophys. Res.*, **91**, 13 892–13 901.
- Steinle-Neumann, G., Stixrude, L., Cohen, R.E. & Gülseren, O., 2001. Elasticity of iron at the temperature of the Earth's inner core, *Nature*, **413**, 57–60.
- Su, W.-J. & Dziewonski, A.M., 1995. Inner core anisotropy in three dimensions, *J. geophys. Res.*, **100**, 9831–9852.
- Tanaka, S. & Hamaguchi, H., 1997. Degree one heterogeneity and hemispherical variation of anisotropy in the inner core from *PKP(BC)*–*PKP(DF)* times, *J. geophys. Res.*, **102**, 2925–2938.
- Tkalčić, H., Romanowicz, B. & Houy, N., 2002. Constraints on *D'* structure using *PKP(AB-DF)*, *PKP(BC-DF)* and *PcP–P*-travel time data from broadband records, *Geophys. Res. Lett.*, **149**, 599–616.
- Tromp, J., 1993. Support for anisotropy of the Earth's inner core from free oscillations, *Nature*, **366**, 678–681.
- Tromp, J., 2001. Inner-core anisotropy and rotation, *Annu. Rev. Earth planet. Sci.*, **29**, 47–69.
- Van der Hilst, R.D., Widiyantoro, S. & Engdahl, E.R., 1997. Evidence for deep mantle circulation from global tomography, *Nature*, **386**, 578–584.
- Vidale, J.E. & Earle, P.S., 2000. Fine-scale heterogeneity in the Earth's inner core, *Nature*, **404**, 273–275.
- Weber, M., 1990. Subduction zones, their influence on travel times and amplitudes of *P*-waves, *Geophys. Res. Lett.*, **101**, 529–544.
- Wen, L. & Niu, F., 2002. Seismic velocity and attenuation in the top of the Earth's inner core, *J. geophys. Res.*, **107**(B11), 2273, 10.1029/2001JB000 170.
- Woodhouse, J.H., Giardini, D. & Li, X.-D., 1986. Evidence for inner core anisotropy from splitting in free oscillation data, *Geophys. Res. Lett.*, **13**, 1549–1552.